

Article

Estimation of Groundwater Evapotranspiration of Different Dominant Phreatophytes in the Mu Us Sandy Region

Wuhui Jia ¹, Lihe Yin ^{2,*}, Maosheng Zhang ³, Kun Yu ², Luchen Wang ^{1,2} and Fusheng Hu ¹

¹ School of Water Resources and Environment, China University of Geosciences, Beijing 100083, China; jiawh@cugb.edu.cn (W.J.); wangluchen@cugb.edu.cn (L.W.); 1991010439@cugb.edu.cn (F.H.)

² Xi'an Center of Geological Survey, China Geological Survey, Xi'an 710054, China; yukun01@mail.cgs.gov.cn

³ Institute of Disaster Prevention and Ecological Restoration, Xi'an Jiaotong University, Xi'an 710049, China; xjtzms@xjtu.edu.cn

* Correspondence: ylihe@cgs.cn; Tel.: +86-29-8782-1680

Abstract: Groundwater evapotranspiration (ET_G) estimation is an important issue in semiarid areas for groundwater resources management and environmental protection. It is widely estimated by diurnal water table fluctuations. In this study, the ET_G at four sites with different plants was estimated using both diurnal water table and soil moisture fluctuations in the northeastern Mu Us sandy region, in order to identify the groundwater utilization strategy by different dominant phreatophytes. Groundwater level was monitored by ventilatory pressure transducers (Solinst LevelVent, Solinst Canada Ltd.; accuracy ± 3 mm), while soil moisture was monitored using EM50 loggers (Decagon Devices Inc., Pullman, USA) in K1 and K14 and simulated by Hydrus-1D in other observation wells. A significant spatial variation of ET_G was found within a limited area, indicating a poor representativeness of site ET_G for regional estimation. The mean values of ET_G are 4.01 mm/d, 6.03 mm/d, 8.96 mm/d, and 12.26 mm/d at the *Achnatherum splendens* site, *Carex stenophylla* site, *Salix psammophila* site and *Populus alba* site, respectively, for the whole growing season. ET_G is more sensitive to depth to water table (DWT) in the *Carex stenophylla* site than in the *Achnatherum splendens* site for grass-dominated areas and more sensitive to DWT in the *Populus alba* site than in *Salix psammophila* site for tree-dominated areas. Groundwater extinction depths are estimated at 4.1 m, 2.4 m, 7.1 m, and 2.9 m in the *Achnatherum splendens* site, *Carex stenophylla* site, *Salix psammophila* site and *Populus alba* site, respectively.

Keywords: diurnal fluctuations; Phreatophyte; semiarid; wetland; vegetation restoration



Citation: Jia, W.; Yin, L.; Zhang, M.; Yu, K.; Wang, L.; Hu, F. Estimation of Groundwater Evapotranspiration of Different Dominant Phreatophytes in the Mu Us Sandy Region. *Water* **2021**, *13*, 440. <https://doi.org/10.3390/w13040440>

Academic Editors: Mirko Castellini, Simone Di Prima, Ryan Stewart, Marcella Biddoccu, Mehdi Rahmati and Vincenzo Alagna

Received: 7 January 2021

Accepted: 4 February 2021

Published: 8 February 2021

Publisher's Note: MDPI stays neutral with regard to jurisdictional claims in published maps and institutional affiliations.



Copyright: © 2021 by the authors. Licensee MDPI, Basel, Switzerland. This article is an open access article distributed under the terms and conditions of the Creative Commons Attribution (CC BY) license (<https://creativecommons.org/licenses/by/4.0/>).

1. Introduction

In arid and semi-arid areas, restoring and protecting the environment is a huge project for the benefit of mankind [1]. While groundwater is a crucial source of ecological restoration because of the lower precipitation and higher evapotranspiration in arid regions. However, these areas also depend heavily on groundwater for industry, drinking water supply and agriculture [2,3]. Reasonable allocation of groundwater resources in all sectors is thus a major environmental issue.

Groundwater is a main water source for phreatophytes in arid and semiarid areas. Evapotranspiration partitioning shows that transpiration accounts for the majority of evapotranspiration [4,5]. Over the past few decades, vegetation coverage has displayed a large increase because of the multiple ecological restoration programs including the grain for green and afforestation in some arid areas of China [6]. However, ecological restoration by afforestation may increase groundwater depth and create potentially large ecological and water costs in arid and semiarid [7]. For example, Gribovszki et al. [8] found that the water table beneath forest was 0.4–0.5 m lower than that beneath grassland due to the afforestation in the Hungarian Great Plain. So, the groundwater consumption strategy of each phreatophyte should be considered in the process of afforestation.

In addition, groundwater evapotranspiration (ET_G) is a vital factor for groundwater balance analysis in arid and semi-arid regions. For example, almost 60% of natural groundwater discharge is through ET_G in the Ordos Plateau in NW China [9]. Many studies usually estimate ET_G indirectly, i.e., by the pan coefficient method [10], the remote sensing method [11] and the eddy covariance method [12]. The pan coefficient method is simple, but coefficients mainly are empirical with low precision. The remote sensing method is usually used to calculate evapotranspiration at a regional scale and the time step depends on remote sensing data. It cannot analyze the temporal and spatial variation of evapotranspiration at small scale. The eddy covariance method depends on expensive instruments, so it is not widely used. In addition, all of these methods estimate rather total evapotranspiration than ET_G . Evapotranspiration partitioning is needed to exclude the contribution of soil water, which is a complicated process. Therefore, over the past few decades, the method of estimating evapotranspiration based on diurnal water table fluctuations, developed by White [13], has attracted more and more attention [14–18], because it can estimate ET_G directly with fewer parameters and lower costs.

The Mu Us sandy region is a part of the Ordos Plateau in NW China and is used to be one of the most seriously desertified areas in China [19]. It has also undergone a significant vegetation restoration in recent decades [20]. While Cheng et al. [21] estimated the ET_G at four sites in the center of the Mu Us sandy region, using only one observation at each site. However, the spatial variation of ET_G at point scale under each vegetation is unclear and the representativeness of the ET_G for one observation well is also uncertain. Multiple wells are expected to improve the accuracy of ET_G estimation in each vegetation site [22]. Therefore, the objectives of this study are (1) to estimate the ET_G from multiple observation wells based on the water table and soil moisture fluctuations at different sites; (2) to study the temporal and spatial variations of ET_G ; and (3) to analyze the sensitivity of ET_G of different vegetation to water table depth.

2. Materials and Methods

2.1. Site Description

The study site ($39^{\circ}16'54''\sim 39^{\circ}18'48''$ N, $108^{\circ}47'40''\sim 108^{\circ}50'03''$ E) is located in the northeastern Mu Us sandy region, within a wetland of the Mukai Lake in Ordos City, Inner Mongolia, NW China. The geomorphology is mainly lake basin that contains some microrelief, such as wetlands, crescent sand dunes, and highlands (Figure 1). Vegetation is distributed unevenly in the various microrelief. Vegetation coverage is higher in wetlands, up to about 70%. While, there is only sparse vegetation on sand dunes. The climate is semi-arid characterized by a low rainfall and high evapotranspiration. According to the long-term meteorological data (2000–2017) from the Wushenzhao meteorological station near the study area, the mean annual precipitation is ~ 330 mm and over 70% of the annual precipitation falls from June to September. Average reference evapotranspiration (ET_0) calculated by the Penman–Monteith equation [23] is ~ 1150 mm/a. Average annual air temperature is about 7.0 °C, with a maximum of 22.4 °C in July and a minimum of -11.0 °C in January. Population density is low and arable lands near the study area are scarce, so the consumption of groundwater by human activities is negligible.

The main species of vegetation are *Achnatherum splendens* (Figure 2a), *Carex stenophylla* (Figure 2b), *Populus alba* (Figure 2c), *Salix psammophila* (Figure 2d), and *Caragana korshinskii* (Figure 2e). The grass sites (*Achnatherum splendens* and *Carex stenophylla*) are distributed around the lake, while the tree sites (*Populus alba*, *Salix psammophila* and *Caragana korshinskii*) are located adjacent and upstream of the grass sites.

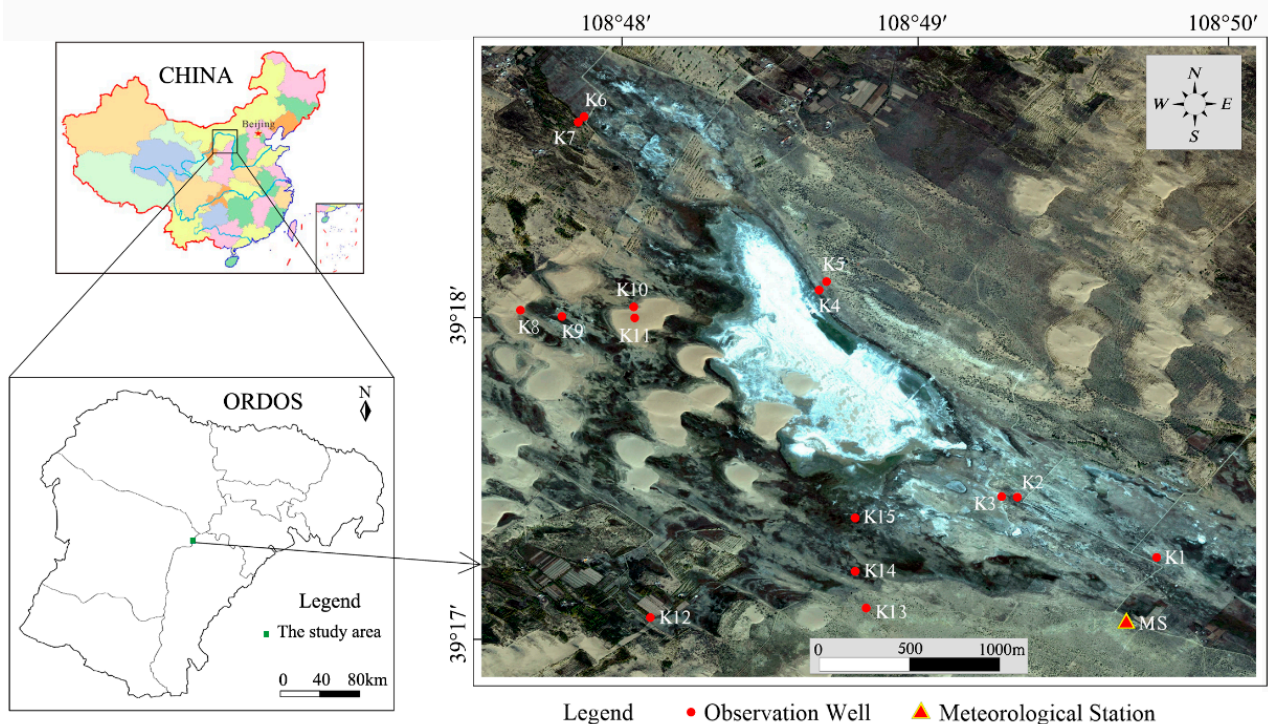


Figure 1. Location map of the study site showing the observation wells and meteorological station.

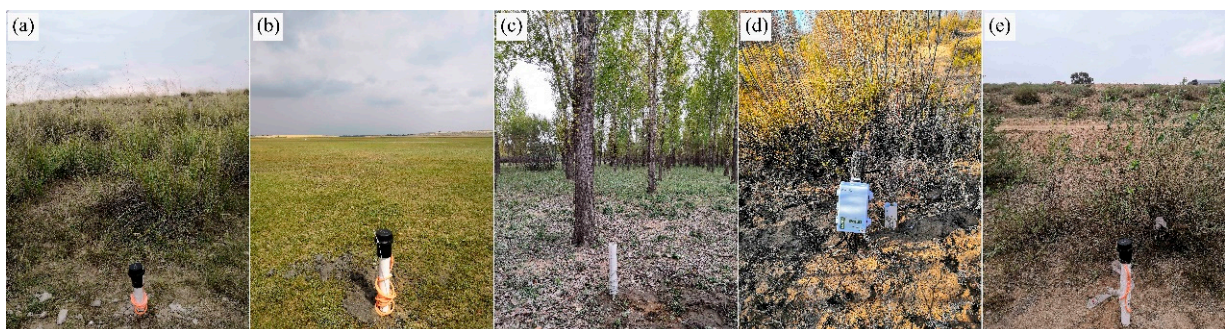


Figure 2. The dominate vegetations, i.e., (a) *Achnatherum splendens*, (b) *Carex stenophylla*, (c) *Populus alba*, (d) *Salix psammophila* and (e) *Caragana korshinskii*, in the study site.

2.2. Monitoring Design

Fifteen shallow observation wells (K1 to K15) were drilled by a hand auger around the lake (Figure 1). K1, K2, and K3 are in the *Achnatherum splendens* site; K4, K9, K10, K14, and K15 are in the *Carex stenophylla* site; K5 and K13 are in the *Caragana korshinskii* site; K6, K7 are in the *Salix psammophila* site; K8 and K11 are located in sand dunes; K12 is in the *Populus alba* site. The depth of the wells varies between 2 m and 4 m, depending on the depth to water table (DWT) at each site. Each was constructed using a 50 mm PVC pipe screened over the entire subsurface length. Augured soil was backfilled around the PVC pipe and granular bentonite was then packed around land surface to avoid preferential flow.

Groundwater level was continuously monitored from 1 April 2019 to 31 October 2019 at one-hour intervals by ventilatory pressure transducers with data logging capability (Solinst LevelVent, Solinst Canada Ltd.; accuracy ± 3 mm) that automatically eliminated the effect of air pressure fluctuations by a vented cable to the wellhead. The well cap assembly of the transducers serves to prevent direct rainfall input and evaporation loss. In order to remove noise, a five-point moving average was used to smoothen groundwater level

data [18]. The data were also calibrated frequently in the field with manual measurements of DWT.

Soil samples were collected from different depths and the particle sizes were determined by the sieving method for the sand fractions and by a soil hydrometer for the silt and clay fractions. Results showed that the soil texture of unsaturated zone at the study sites was mainly fine sand and homogeneous in the vertical direction at each well (Table 1). The soil textures of all observation wells were divided artificially into two categories, with sand content higher than 90%, and with sand content less than 90%. Then, two observation sites, K1 and K14, were thought to be representative of the two soil textures. Soil moisture (θ_s) was monitored once an hour from 20 cm to 100 cm below ground surface with 20 cm intervals at K1 and from 20 cm to 60 cm with 10 cm intervals at K14 using EM50 loggers (Decagon Devices Inc., Pullman, USA).

Table 1. Particle size distribution at different depths in the Observation wells.

Wells	Soil Depth (cm)	Sand (%)	Silt (%)	Clay (%)
K1	40	82.9	17.1	0
	60	83.4	16.6	0
	80	86.3	13.7	0
K3	50	85.0	15.0	0
	70	85.1	14.9	0
K4	20	85.5	14.5	0
	50	83.2	16.8	0
	70	81.9	18.1	0
K6	50	91.0	9.0	0
	80	91.1	8.9	0
K9	20	85.6	14.4	0
	50	85.2	14.8	0
K10	20	92.7	7.3	0
	50	94.7	5.3	0
K12	50	92.4	7.6	0
	80	92.9	7.1	0
	100	95.7	4.3	0
K14	30	98.0	2.0	0
	60	98.4	1.6	0
	80	92.6	7.4	0
K15	20	87.2	12.8	0

Meteorological data (i.e., solar radiation, air temperature, air humidity, and wind speed) were monitored at one-hour intervals by a meteorological station (HOBO-U30, Onset, USA) at the southeast of study site. Hourly reference evapotranspiration (ET_0) was calculated by the Penman–Monteith Equation (Equation (1)) using the meteorological data [23].

$$ET_0 = [0.408\Delta(R_n - G) + 37\gamma\mu(e^\circ(T_h) - e_a)/(T_h + 273)]/[\Delta + \gamma(1 + 0.34\mu)]. \quad (1)$$

where ET_0 is reference evapotranspiration ($\text{mm}\cdot\text{h}^{-1}$); R_n is net radiation ($\text{MJ}\cdot\text{m}^{-2}\cdot\text{h}^{-1}$); G is soil heat flux density ($\text{MJ}\cdot\text{m}^{-2}\cdot\text{h}^{-1}$); T_h is mean hourly air temperature ($^\circ\text{C}$); Δ is saturation slope vapor pressure curve at T_h ($\text{kPa}\cdot^\circ\text{C}^{-1}$); γ is psychrometric constant ($\text{kPa}\cdot^\circ\text{C}^{-1}$); $e^\circ(T_h)$ is saturation vapor pressure at air temperature T_h (kPa); e_a is average hourly actual vapor pressure (kPa); μ is average hourly wind speed ($\text{m}\cdot\text{s}^{-1}$). It is worth noting that ET_0 is the evapotranspiration from the reference surface which is under a hypothetical grass reference crop with an assumed crop height of 0.12 m, a fixed surface resistance of $70\text{ s}\cdot\text{m}^{-1}$ and an albedo of 0.23. The reference surface closely resembles an extensive surface of green,

well-watered grass of uniform height, actively growing and completely shading the ground. The fixed surface resistance of $70 \text{ s}\cdot\text{m}^{-1}$ implies a moderately dry soil surface resulting from about a weekly irrigation frequency [23].

2.3. Numerical Simulations

2.3.1. Soil Hydraulic Parameters Estimated by Inverse Modeling

Soil hydraulic parameters were obtained through inverse modeling by Hydrus-1D, which was widely used by previous studies [24–26]. For K1 and K14, as the representative of the two soils, both groundwater level and soil moisture were monitored. Therefore, the meteorological data, water table and soil moisture data were used to inverse soil hydraulic parameters of the two soil textures in the study site.

For the inverse modeling, a 150 cm homogeneous soil profile was divided uniformly into 150 elements, with 151 nodes and two observations corresponding to the soil moisture monitoring depths (20 cm and 100 cm at K1; 20 cm and 40 cm at K14). The maximum number of iterations was set to 50. The van Genuchten–Mualem hydraulic model was selected and the soil hydraulic parameters of loamy sand in the model were used as the initial parameters because the soil texture is classified as loamy sand based on particle size analysis. The maximum and minimum values of each parameter, i.e., θ_r , θ_s , φ , n , and K_s , are set to limit the range of inversion. According to the particle analysis of soils in the study site (Table 1), the maximum values of φ , n and K_s were set to the default parameters of sand in Hydrus-1D code and the minimum values equaled to the default parameters of silt, as shown in Table 2. Data for inverse solution were soil moisture data measured in the field at the two observations depths. Time discretization was in hours and initial time step was set to 0.01.

Table 2. The initial, minimum and maximum values of the soil hydraulic parameters in inverse solution.

	θ_r (cm^3/cm^3)	θ_s (cm^3/cm^3)	φ (1/cm)	n	K_s (cm/h)
Initial Value	0.057	0.41	0.124	2.28	14.5917
Minimum	0	0	0.016	1.37	0.25
Maximum	0.078	0.43	0.145	2.68	29.7

The upper boundary condition was defined as an atmospheric boundary condition. The potential evapotranspiration (ET_p) equals to ET_0 as recommended by Šimůnek et al. [27], and the potential evaporation (E_p) and potential transpiration (T_p) were estimated from ET_p using Beer’s law that partitions the solar radiation component of the energy budget via interception by the canopy [28,29] as follows in Equations (2) and (3):

$$E_p = ET_p \times e^{-k \cdot LAI} \quad (2)$$

$$T_p = ET_p \times (1 - e^{-k \cdot LAI}) \quad (3)$$

where k is a constant governing the radiation extinction by the canopy (-), the value is about 0.6 according to Belmans et al. [30]. LAI is the leaf area index and the values in grass site and tree site are 1.9 and 2.6, respectively. The lower boundary condition was variable pressure head that was monitored in the study site. The period of the inverse model was from 20 May 2019 to 5 June 2019 for K1 and from 24 May 2019 to 6 September 2019 for K14, when obvious diurnal fluctuations of water table and soil water moisture continuously occurred.

In the study site, the root depth was about 150 cm. An exponential root distribution model developed by Zeng [31] was used in our model, as follow in Equation (4):

$$Y = 1 - 0.5 (e^{-ad} + e^{-bd}) \quad (4)$$

where Y is the cumulative root fraction from the surface to depth d ; a and b are the empirical coefficients. For short grass, a and b are 10.74 and 2.61, respectively. The S-shaped water stress function of root water uptake was adopted [32].

2.3.2. Simulated Soil Moisture

Soil moisture was monitored at K1 and K14 and simulated by Hydrus-1D at other observation wells, because of the lack of monitoring equipment. The simulation domain is a 150 cm homogeneous soil profile and was divided uniformly into 150 elements with 151 nodes. The simulated period was from 1 April 2019 to 31 October 2019 and the soil hydraulic parameters were from the above-mentioned inverse modelling. The upper boundary condition was also atmospheric boundary condition. E_p and T_p were also estimated by Equations (2) and (3). The lower boundary condition was also defined as a variable pressure head condition. Root depth was 150 cm in the grass site and 200 cm in the areas with arboreous vegetation. The root water uptake model and root distribution model are same to the models used in the previous section. While the parameters a and b in the root distribution model are 7.07 and 1.95, respectively, for deciduous needleleaf tree, i.e., *Salix psammophila*, and are 5.99 and 1.96, respectively, for deciduous broadleaf tree, i.e., *Populus alba*, according to Zeng [31]. The observation points were set from the land surface to water table with 10 cm intervals to obtain soil moisture along the soil profile. To test the accuracy of the simulated data, the soil moisture of K1 (60 cm and 80 cm depth) and K14 (50 cm and 70 cm depth) were also simulated and then compared to the measured data.

2.3.3. Statistical Analysis

The root mean square error (RMSE), Nash–Sutcliffe efficiency (NSE) and percent bias (PBIAS) were used to compare the observed and simulated soil moisture. They are defined as Equations (5)–(7), respectively, as followed:

$$\text{RMSE} = \sqrt{[\sum_i^n (\theta_{\text{obs},i} - \theta_{\text{sim},i})^2] / n} \quad (5)$$

$$\text{NSE} = 1 - \frac{\sum_i^n (\theta_{\text{obs},i} - \theta_{\text{sim},i})^2}{\sum_i^n (\theta_{\text{obs},i} - \text{ave}\theta_{\text{obs},i})^2} \quad (6)$$

$$\text{PBIAS} = 100 \times [\sum_i^n (\theta_{\text{sim},i} - \theta_{\text{obs},i}) / \sum_i^n \theta_{\text{obs},i}] \quad (7)$$

where θ_{obs} is the observed soil moisture in field, θ_{sim} is the simulated soil moisture, n is the number of observations, $\text{ave}\theta_{\text{obs}}$ is the average soil moisture of all the observed events.

RMSE indicates the degree of dispersion of the simulated soil moisture relative to the observed moisture [33], and a higher value indicates a higher error in the simulated moisture. NSE represents the extent to which the simulated moisture and the observed moisture follow a 1:1 slope line [34]. It ranges from $-\infty$ to 1 and higher values indicate a better agreement with the observed moisture [35]. PBIAS measures the average tendency of the simulated values to be larger or smaller than their observed ones. The optimal value of PBIAS is 0.0, with small values indicating accurate model simulation. Positive values indicate overestimation bias, and negative values indicate model underestimation bias.

2.4. ET_G Estimation

White [13] initially developed a method to quantify daily ET_G using diurnal water table fluctuations (hereafter referred to as the White method [36]), as follows in Equation (8):

$$ET_G = S_y \times (24r \pm s) \quad (8)$$

where ET_G is the daily groundwater evapotranspiration ($L \cdot T^{-1}$), S_y is the specific yield of sediments ($-$), r is the rate of water table recovery during nighttime ($L \cdot T^{-1}$) and s is the daily change in storage ($L \cdot T^{-1}$)

In this study, a modified White method was adopted to estimate the daily ET_G . For the method, daily hydrostatic equilibrium recovery (R_e) is proposed to correct the groundwater inflow estimated by the White method, taking the disequilibrium of soil

water into consideration. The hydrostatic equilibrium at the capillary zone is disturbed at the moment when root water uptake commences in the morning, then the degree of deviation from hydrostatic equilibrium increases in daytime due to the higher ET rate than the hydrostatic equilibrium recovery rate. So, capillary water continues to be replenished by groundwater to lower the degree of deviation from hydrostatic equilibrium at night, resulting in groundwater inflow being underestimated by water table recovery in the White method. Thus, daily R_e is estimated by extending the capillary water recovery rate at nighttime to the whole day, representing the error of daily groundwater inflow estimated by the White method. The procedure for calculating R_e is quite similar to that of the recovery rate (r in Equation (8)) in the White method. The first step is the calculation of the deviation of total soil water (TSW) from hydrostatic equilibrium, $(TSW_{eq} - TSW_s)$, at two specified times (i.e., 22:00 and 6:00 in this study) during nighttime, respectively, then the difference between $(TSW_{eq} - TSW_s)$ of both points of time is determined, and finally the daily R_e is calculated by multiplying by 24 h. Equations (9) and (10) are the mathematical expressions for R_e :

$$R_e = 24 \times [(TSW_{eq} - TSW_s)_t - (TSW_{eq} - TSW_s)_{t+\Delta t}] / \Delta t \quad (9)$$

and

$$TSW = \int_d \theta dz = \sum_j^d 0.5 \times (Z_{j+1} - Z_j) \times (\theta_{j+1} + \theta_j) \quad (10)$$

where TSW_{eq} is the TSW in the column for the corresponding DWT under hydrostatic equilibrium conditions (L); TSW_s is the TSW computed from the field measured water content values (L); θ is water content ($L^3 \cdot L^{-3}$); j is the soil moisture monitoring point of the soil column. Then the daily ET_G was estimated as follows in Equation (11):

$$ET_G = S_y (24r \pm s) + R_e \quad (11)$$

The soil moisture under a hydrostatic equilibrium condition was calculated using the van Genuchten soil water retention properties (Equations (12) and (13)).

$$\theta(h) = \theta_r + (\theta_s - \theta_r) / [1 + (\varphi |h|)^n]^m, h < 0 \quad (12)$$

$$\theta(h) = \theta_s, h \geq 0 \quad (13)$$

where h is the water pressure head (L), θ_s and θ_r are the saturated and residual soil moisture ($L^3 \cdot L^{-3}$), respectively, φ is the air entry value also referred as bubble pressure (L^{-1}), n is the pore size distribution parameter ($-$), $m = 1 - 1/n$ ($-$), and φ , n , and m are the empirical shape factors in the water retention function.

It should be noted that specific yield (S_y) is the most crucial factor for ET_G estimation by water table fluctuations [37–39]. S_y is defined as the volume of water released under gravity from storage per unit cross sectional area per unit decline in water table [40]. It is affected by soil texture, depth to water table and drainage time [38]. So, the depth-dependent and time-dependent S_y are widely used to estimate ET_G based on water table fluctuations [21,37].

In this study, the drainage time is not taken into account because the change of capillary water has been calculated. Therefore, the equation for depth-dependent S_y developed by Duke [41] with van Genuchten parameters was used (Equation (14))

$$S_y = \theta_s - [\theta_r + (\theta_s - \theta_r) / [1 + (\varphi |d|)^n]^m] \quad (14)$$

where d is the depth to water table (L).

3. Results and Discussion

3.1. Soil Hydraulic Parameters

The measured and simulated soil moisture from inverse modelling at two depths for each observation well (K1 and K14) are shown in Figure 3. The RMSE, NSE, PBIAS, and R-square (R^2) of measured and simulated data were $0.003 \text{ cm}^3/\text{cm}^3$, 0.99, -0.04% , and 0.99, respectively, for K1, while for K14, the RMSE, NSE, PBIAS, and R^2 of measured and simulated data were $0.015 \text{ cm}^3/\text{cm}^3$, 0.86, 1.22%, and 0.81, respectively. According to the statistical analysis, the simulated soil hydraulic parameters of K1 and K14, as showed in Table 3, were a good representation of the actual field parameters.

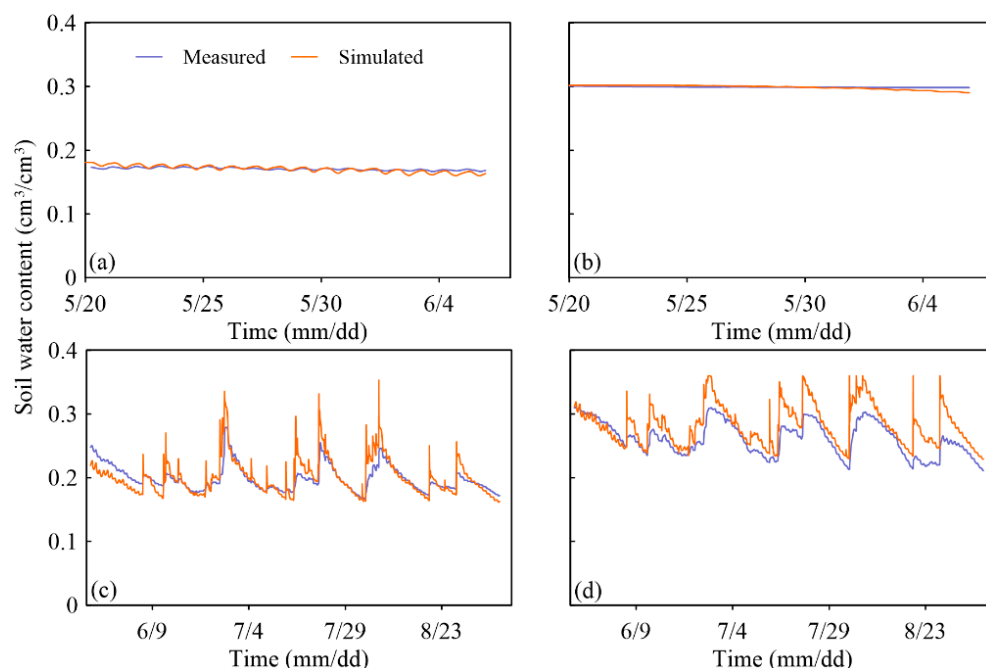


Figure 3. The measured and simulated data of soil moisture at (a) 20 cm depth and (b) 100 cm depth for K1, and (c) 20 cm depth and (d) 40 cm depth for K14.

Table 3. Simulated soil hydraulic parameters for K1 and K14.

Well	$\theta_r \text{ (cm}^3/\text{cm}^3)$	$\theta_s \text{ (cm}^3/\text{cm}^3)$	$\phi \text{ (1/cm)}$	n	$K_s \text{ (cm/h)}$
K1	0.0453	0.302	0.0253	1.78	14.2
K14	0.0532	0.387	0.0282	2.68	29.4

3.2. Validation of the Simulated Soil Moisture

Soil moisture was also simulated at K1 and K14 to assess the accuracy of the modelled soil moisture, using the measured and simulated soil moisture at 60 cm and 80 cm for K1 and 50 cm and 70 cm for K14. As shown in Figure 4 and Table 4, the simulated soil moisture has a good agreement with the measured data, with the mean RMSE of $0.012 \text{ cm}^3/\text{cm}^3$ at K1 and $0.019 \text{ cm}^3/\text{cm}^3$ at K14. While the NSE and R^2 at K14 are 0.25 and 0.21, respectively. The possible reason is that the sensitivity of the monitoring instrument decreases due to the observation depth being close to water table.

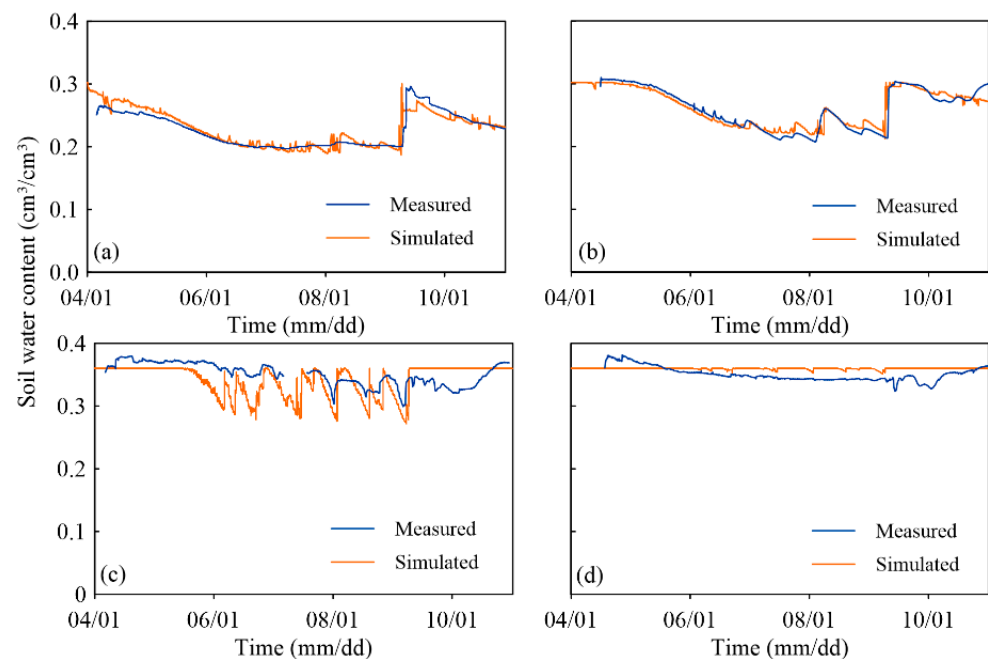


Figure 4. The measured and simulated data of soil moisture at (a) 60 cm depth and (b) 80 cm depth for K1, and (c) 50 cm depth and (d) 70 cm depth for K14.

Table 4. The root mean square error (RMSE), Nash-Sutcliffe efficiency (NSE), percent bias (PBIAS) and R-square (R^2) of the measured and simulated soil moisture for K1 and K14.

	RMSE (cm^3/cm^3)	NSE	PBIAS (%)	R^2
K1	0.012	0.88	0.18	0.89
K14	0.019	0.25	−1.82	0.21

3.3. Temporal and Spatial Variations of Water Table

Obvious diurnal water table fluctuation occurred during the whole growing season in the field. As shown in Figure 5a and b, groundwater table fell during daytime and recovered during nighttime. The variation pattern of water table at sub-daily scale is mainly caused by the evapotranspiration of vegetation. While solar radiation is a dominant factor controlling plant water use in sub-daily scale [42,43], and further influences water table variations (Figure 5c).

The changes in water table at seasonal scales are reflected in daily amplitudes. For the *Carex stenophylla* site, the average daily amplitudes of water table at K10 are 1.7 cm, 2.3 cm, and 1.4 cm in the early, middle, and late of the growing season, respectively (Figure 5a). While they are 2.3 cm, 4.1 cm, and 1.3 cm, respectively, at K12 in the *Populus alba* site (Figure 5b). Obviously, the daily amplitude of water table in the middle of the growing season is larger than that in the early and late of the growing season. It is mainly caused by the vegetation vitality that depends on air temperature (Figure 5d).

The patterns of water table fluctuation in the field are also different for various DWT. In the *Achnatherum splendens* site, the mean daily amplitude of water table is 0.2 cm with an average DWT of 1.85 m at K2 from 21 May to 25 May (Figure 6a). At K3, the mean daily amplitude of water table is 0.6 cm with an average DWT of 0.71 m in the same period. In addition, the mean daily amplitude of water table at K6 and K7 are 5.8 cm and 1.8 cm with average DWT of 0.99 m and 1.67 m, respectively, from 1 July to 5 July in the *Salix psammophila* site (Figure 6b). Obviously, the daily amplitude of water table with shallow water table is larger than that with deep water table in the same vegetation condition,

mainly resulting from the decrease of root distribution and increase of specific yield with DWT.

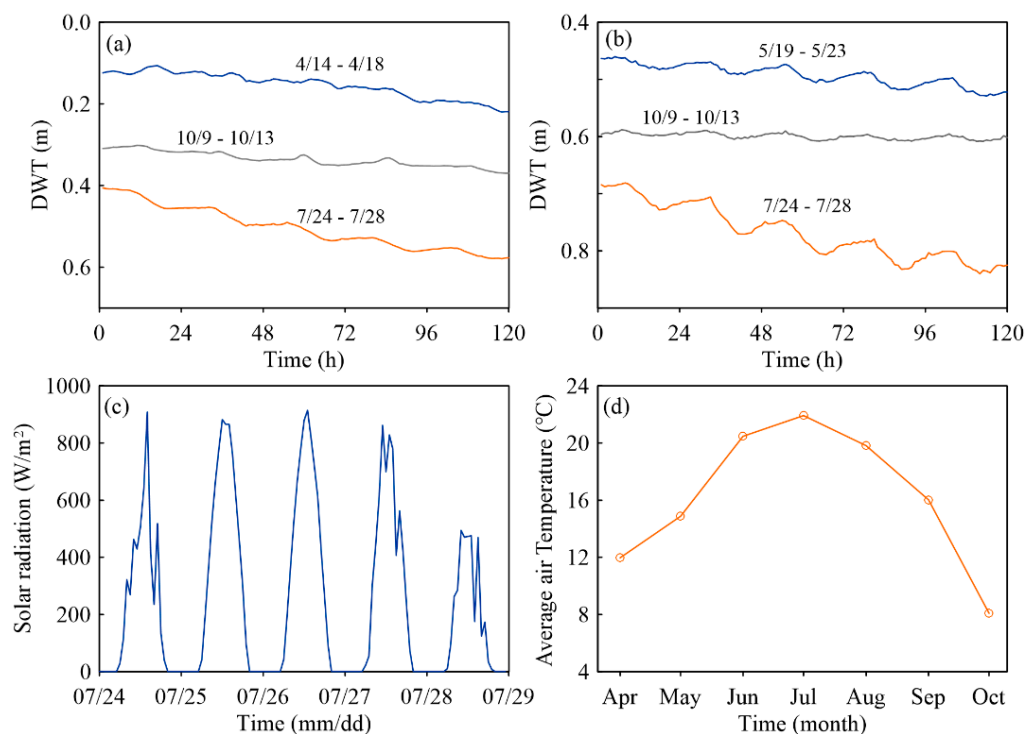


Figure 5. The depth of water table (DWT) of K10 (a) and K12 (b) at the different periods of the growing season; (c) the variation of hourly solar radiation during 24 to 28 July and (d) monthly average air temperature.

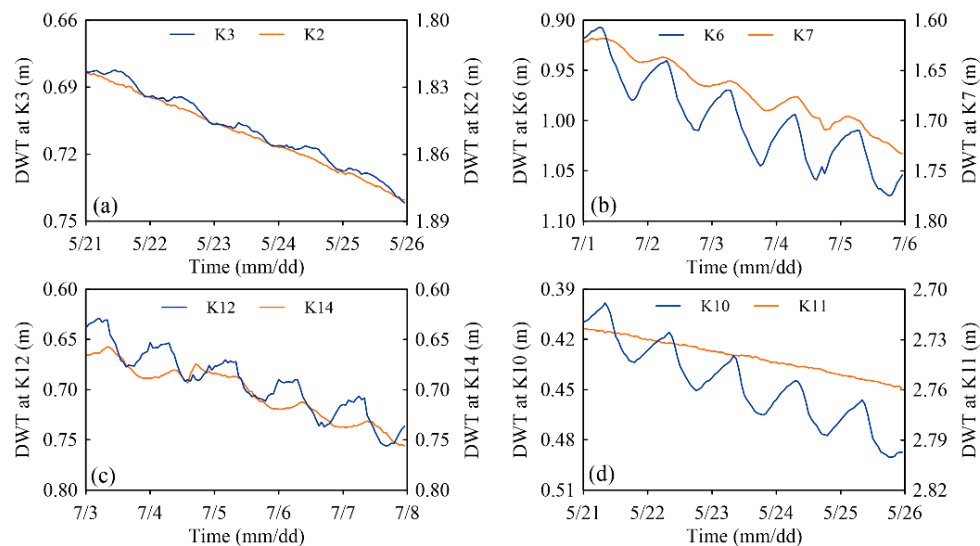


Figure 6. The water table fluctuations vary with (a) the DWT in *Achnatherum splendens* site and (b) the DWT in *Salix psammophila* site, (c) the vegetation conditions in the same DWT, and (d) the microrelief.

Vegetation condition is also a vital influencing factor of water level fluctuation pattern. For example, the daily amplitude of water table (3.7 cm) at K12 in the *Populus alba* site is larger than that (2.0 cm) at K14 in the *Carex stenophylla* site with the same average DWT of 0.70 m (Figure 6c). Furthermore, K10 is in the *Carex stenophylla* site and a sand dune at a distance of 20 m from K10 is free of vegetation. There is obviously water table fluctuation at K10 but no water table fluctuation at K11 (Figure 6d). The water table shows no fluctuation

at K5 and K13 either, indicating that water table fluctuation is not influenced by other factors, such as tidal [44,45] and barometric pressure [46].

3.4. Groundwater Evapotranspiration

3.4.1. Temporal Variations of ET_G

ET_G was estimated except for the wells with no diurnal water table fluctuations, i.e., K5, K11, and K13, indicating that *Caragana korshinskii* is a plant independent of groundwater. There were no ET_G data on rainy days due to the inapplicability of the estimated method. Average daily ET_G and the standard deviation of ET_G at all the observation wells are showed in Figure 7. Temporal variations of ET_G are obvious in the growing season. The average ET_G is small (1.5 mm/d) in the early April and gradually increases to peak values (10.6 mm/d) at the end of July, then gradually decreases to 3.5 mm/d at the end of October. The variation trend is consistent with daily average air temperature (Figure 7), indicating that seasonal ET_G variation mainly depends on air temperature. However, the higher air temperature corresponds to the lower ET_G in April. It may result from the less vitality of vegetation due to the less leaf area in the early growing season [42].

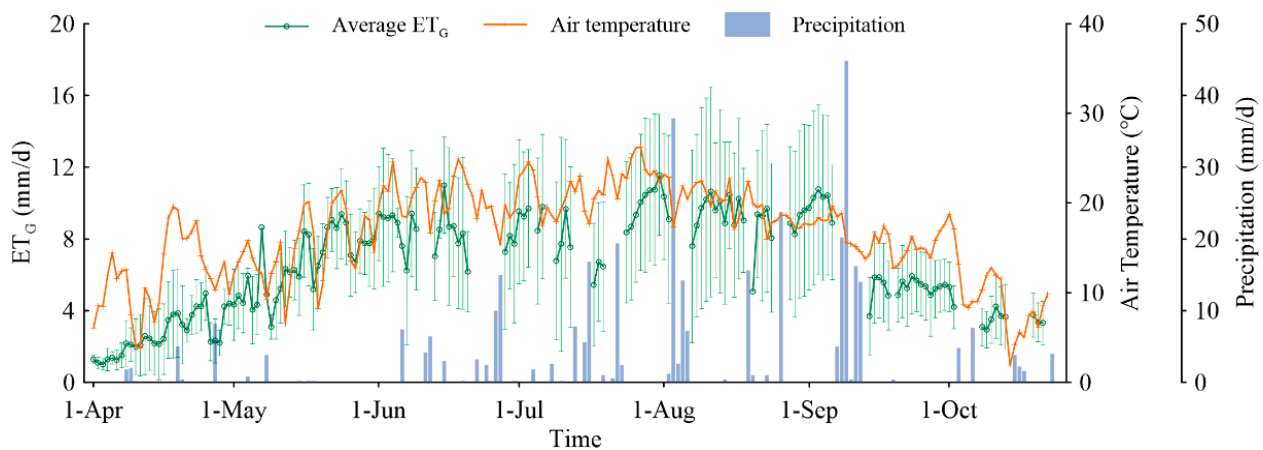


Figure 7. Average groundwater evapotranspiration (ET_G) and the standard deviation of ET_G at all the observation wells with air temperature and precipitation over the growing season.

3.4.2. Spatial Variations of ET_G

Spatial variation is significant indicated by the high standard deviation of the ET_G . The standard deviation shows a similar variation pattern to the average ET_G , which is small in the early and late growing season and large in the middle growing season. The large deviation (4.2 mm/d on average) in the middle of the growing season mainly depends on vegetations types and DWT of the observation wells. For example, the mean ET_G in June was 10.9 mm/d at K12 site with *Populus alba*, which was 1.7 times that of K14 (6.4 mm/d) in the *Carex stenophylla* site with the same average DWT of 0.65 m. On the other hand, the mean ET_G was 2.9 mm/d at K2 site with a mean DWT of 2.03 m and 4.1 mm/d at K3 site with a mean DWT of 0.87 m in June for the *Achnatherum splendens* site. The spatial variations of ET_G were also significant although the distance of two observations was small, for instance, the mean ET_G of K10 was 5.8 mm/d over the growing season in the *Carex stenophylla* site while there was no ET_G at K11 in a sand dune even though it is only 20 m away from K10.

The higher standard deviation of ET_G is also observed from the wells at the same vegetation site (Table 5). The mean standard deviation of average daily ET_G at monthly scale are 1.76 mm/d, 1.89 mm/d, and 3.43 mm/d with the average daily ET_G of 4.01 mm/d, 6.03 mm/d, and 8.96 mm/d in the *Achnatherum splendens* site, *Carex stenophylla* site, and *Salix psammophila* site, respectively. It reflects that the average standard deviation increases with the average ET_G in various vegetation sites.

Table 5. The average groundwater evapotranspiration (ET_G) and standard deviation at monthly scale for various vegetation sites.

	<i>Achnatherum splendens</i> Site		<i>Carex stenophylla</i> Site		<i>Salix psammophila</i> Site	
	Average ET_G (mm/d)	Standard Deviation (mm/d)	Average ET_G (mm/d)	Standard Deviation (mm/d)	Average ET_G (mm/d)	Standard Deviation (mm/d)
Apr-2019	3.11	2.40	2.05	0.86	6.58	0
May-2019	4.07	1.82	6.71	1.48	8.76	1.76
Jun-2019	3.69	2.20	7.75	2.18	10.51	5.60
Jul-2019	4.31	1.32	7.96	2.38	10.70	3.80
Aug-2019	4.54	1.45	7.93	2.58	12.60	5.45
Sep-2019	4.18	1.66	6.07	2.21	9.25	2.31
Oct-2019	3.19	1.49	3.71	1.53	4.29	1.67

The large spatial difference of ET_G at different wells reflects that ET_G estimated by one observation well can only represent point-scale ET_G . However, Butler et al. [42] used a point-scale ET_G to quantify the ET_G of an area of 150 m². According to our analysis, it may cause a large error to study regional ET_G by a point value and the mean ET_G of multiple wells in an area will be more representative, even though in the same vegetation site. Therefore, more observation wells are needed in an area to obtain a region-scale ET_G .

3.4.3. Average ET_G in Different Vegetation Sites

For various vegetations, the average ET_G over the whole growing season (April to October 2019) are 4.01 mm/d, 6.03 mm/d, 8.96 mm/d, and 12.26 mm/d at the *Achnatherum splendens* site, *Carex stenophylla* site, *Salix psammophila* site, and *Populus alba* site with the average DWT of 1.19 m, 0.49 m, 1.30 m, and 0.74 m, respectively. It is obvious that the ET_G in the tree sites is about twice as much as that of the grass sites. The same relationship has been found in previous studies [21,22]. For example, Satchithanatham et al. [22] found that the average ET_G at trees sites and grass sites were 4.1 mm/d and 2.1 mm/d, respectively, in the Assiniboine River drainage basin in southwestern Manitoba, Canada. Although the average ET_G of trees and grass also shows two to one ratio, both of them are much less than that of our study. There are several possible reasons. Firstly, the average DWT in the Assiniboine River drainage basin (1.4 m for trees sites and 1.0 m for grass sites) was larger than that in our study site (1.1 m and 0.5 m for trees and grass sites, respectively). While groundwater absorbed by vegetation decreases with DWT [43]. Secondly, the annual precipitation in the Assiniboine River drainage basin was 474 mm, being 44% larger than that of our study site (330 mm) due to the climate difference. Vegetation will use more soil water from rainfall infiltration than groundwater because the soil water is rich in nutrients and oxygen [47,48]. Finally, the ET_G estimated method in our study considers the daily hydrostatic equilibrium recovery in capillary zones that is considered to be a part of ET_G .

3.4.4. Sensitivity of ET_G to Influencing Factors

ET_0 reflects the combined effect of individual meteorological variables because it is determined by solar radiation, air temperature, relative humidity, and wind speed (Equation (1)). As shown in Figure 8, ET_G has a linear positive correlation with ET_0 in each observation well. The slope of the linear expression of them are considered to be the parameter that reflects the relationship between ET_G and ET_0 , and they are different among the wells. The slope in K6, K7, and K12 are bigger than one (ranging from 1.03 to 1.78), indicating that the daily ET_G in these wells are generally larger than daily ET_0 . The possible explanation is that the vegetation in K6, K7, and K12 are trees that have larger ET_G than grass. While K4 is close to the lake with dense grass, resulting in the larger ET_G . The slope in the other wells ranges from 0.46 to 0.91. It reflects that the proportion of ET_G and ET_0 shows obvious spatial difference. However, the coefficient of determination (R^2) of

the linear expressions is not suitable for all wells, ranging from 0.06 to 0.67, resulting from other factors influencing ET_G . For example, R^2 are 0.06 and 0.08 in K2 and K7, respectively, where DWT is larger.

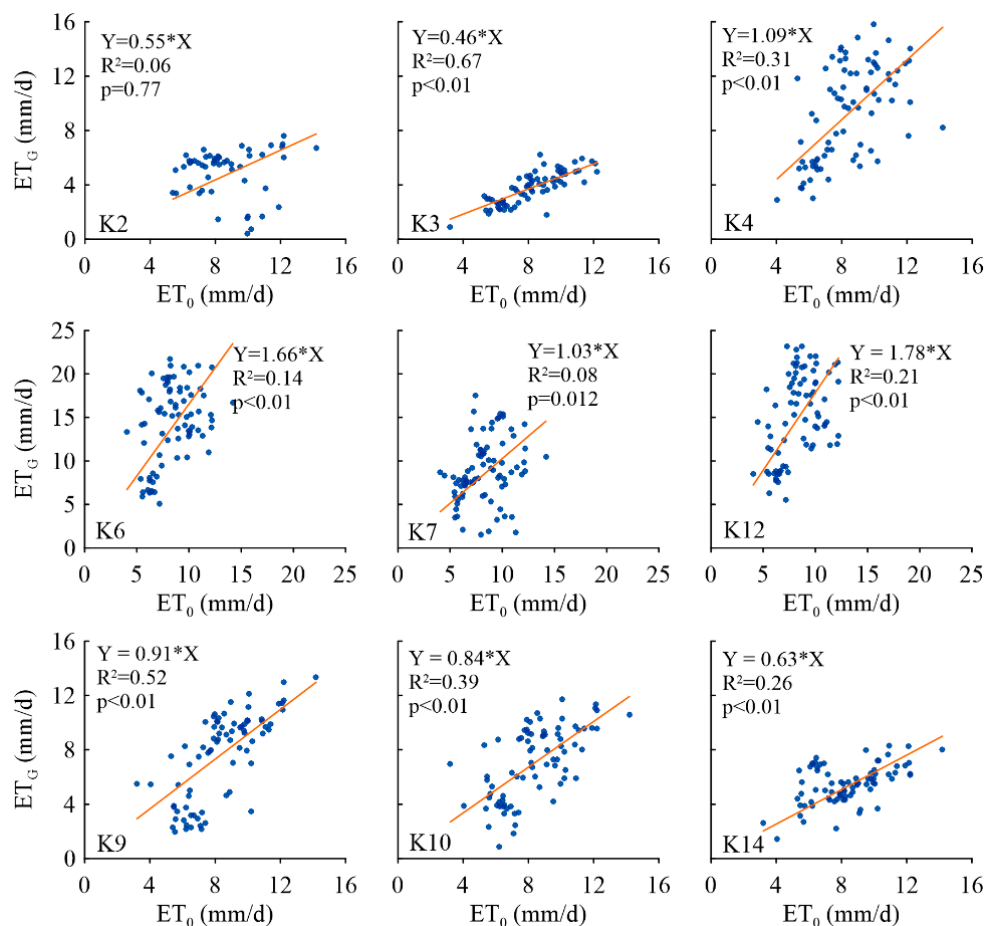


Figure 8. The relationship between ET_0 and ET_G for different observation wells.

In order to obtain the relationship between ET_G and DWT, a ratio of ET_G to ET_0 (ET_G/ET_0) are used to exclude the influence of climatic conditions. For various vegetation types, the exponential decay function between ET_G/ET_0 and DWT are obtained as shown in Figure 9, but the parameters of these functions are different. The maximum ET_G/ET_0 is 1.1 for the grass sites (the *Carex stenophylla* site and the *Achnatherum splendens* site), while the maximum ET_G/ET_0 is 3.6 for the tree sites (the *Populus alba* site and the *Salix psammophila* site), resulted from the larger ET_G in the tree sites. The coefficient of the independent variable (CIV) in the exponential function can reflect the decay rate of the ET_G/ET_0 with DWT. For grass, ET_G/ET_0 decreases more rapidly with DWT in the *Carex stenophylla* site (CIV = -2.35) than in the *Achnatherum splendens* site (CIV = -1.55), indicating that ET_G is more sensitive to DWT in the *Carex stenophylla* site. While ET_G/ET_0 decreases more rapidly with DWT in the *Populus alba* site (CIV = -2.66) than in the *Salix psammophila* site (CIV = -0.98) for the tree sites, suggesting that ET_G in the *Populus alba* site is more sensitive to DWT.

The groundwater extinction depth is assumed to be reached when ET_G/ET_0 decreases to 0.5% [49]. According to the relationship of ET_G/ET_0 and DWT in our study site, the groundwater extinction depth are 4.1 m, 2.4 m, 7.1 m, and 2.9 m in the *Achnatherum splendens* site, *Carex stenophylla* site, *Salix psammophila* site and *Populus alba* site, respectively. It reflects that roots of *Achnatherum splendens* and *Salix psammophila* are deeper and better able to adapt to lower water levels.

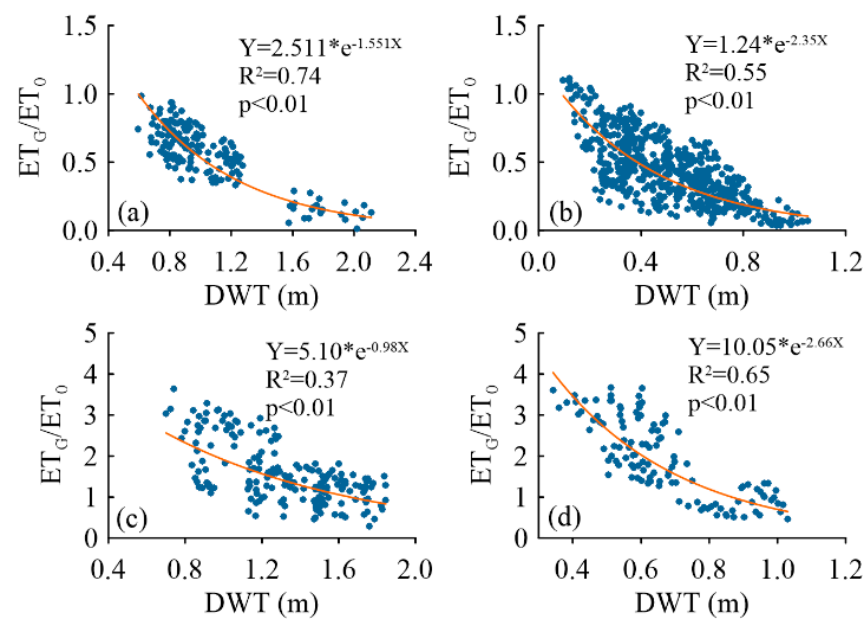


Figure 9. The relationship between the ratio of ET_G to ET_0 (ET_G/ET_0) and DWT for (a) the *Achnatherum splendens* site, (b) the *Carex stenophylla* site, (c) the *Salix psammophila* site, and (d) the *Populus alba* site.

4. Conclusions

In this study, ET_G of four vegetation types was estimated based on the diurnal water table and soil moisture fluctuations in the northeastern Mu Us sandy region. According to the variation of water table fluctuations at multiple wells, the influence of tidal and barometric pressure could be excluded. ET_G in all the observation wells shows a significant temporal and spatial variation in each vegetation site, indicating that the representativeness of ET_G from one observation well is poor and the mean ET_G of multiple wells in an area will be more representative. The average ET_G of multiple observation wells are 4.01 mm/d, 6.03 mm/d, 8.96 mm/d and 12.26 mm/d at the *Achnatherum splendens* site, *Carex stenophylla* site, *Salix psammophila* site, and *Populus alba* site with the average DWT of 1.19 m, 0.49 m, 1.30 m, and 0.74 m, respectively, in the whole growing season.

The main influencing factors of ET_G are ET_0 and DWT. The ET_G is more sensitive to DWT in the *Carex stenophylla* site than that in the *Achnatherum splendens* site for grass sites, and for tree sites, ET_G in the *Populus alba* site is more sensitive to DWT than that in the *Salix psammophila* site, according to the relationship between ET_G/ET_0 and DWT. In addition, the groundwater extinction depths are also predicted to be 4.1 m, 2.4 m, 7.1 m, and 2.9 m in the *Achnatherum splendens* site, *Carex stenophylla* site, *Salix psammophila* site, and *Populus alba* site, respectively. This typical geomorphic unit in the study area is thought to be able to represent the evapotranspiration characteristics of the groundwater-dependent vegetation covered area in the Mu Us Sandy region, northern China.

Author Contributions: Conceptualization, W.J. and L.Y.; methodology, W.J.; software, W.J.; validation, M.Z., F.H. and L.Y.; formal analysis, W.J.; investigation, W.J.; resources, L.Y.; data curation, W.J.; writing—original draft preparation, W.J.; writing—review and editing, L.Y.; visualization, K.Y.; supervision, L.W.; project administration, K.Y.; funding acquisition, L.Y. All authors have read and agreed to the published version of the manuscript.

Funding: This research was funded by China National Natural Science Foundation (41472228 and 41877199), Innovation Capability Support Program of Shaanxi (Program No. 2019TD-040), China Geological Survey (DD20160293), and Key Laboratory of Groundwater and Ecology in Arid Regions of China Geological Survey.

Institutional Review Board Statement: Not applicable.

Informed Consent Statement: Not applicable.

Data Availability Statement: The data presented in this study are available on request from the corresponding author. The data are not publicly available due to privacy.

Acknowledgments: We sincerely acknowledge the anonymous reviewers and the Editor for their useful comments.

Conflicts of Interest: The authors declare no conflict of interest.

References

- Bullock, J.M.; Aronson, J.; Newton, A.C.; Pywell, R.F.; Rey-Benayas, J.M. Restoration of ecosystem services and biodiversity: Conflicts and opportunities. *Trends Ecol. Evol.* **2011**, *26*, 541–549. [\[CrossRef\]](#)
- Mvungi, A.; Mashauri, D.; Madulu, N. Management of water for irrigation agriculture in semi-arid areas: Problems and prospects. *Phys. Chem. Earth Parts A/B/C* **2005**, *30*, 809–817. [\[CrossRef\]](#)
- Alvarez, M.D.P.; Trovatto, M.M.; Hernández, M.A.; Gonzalez, N. Groundwater flow model, recharge estimation and sustainability in an arid region of Patagonia, Argentina. *Environ. Earth Sci.* **2012**, *66*, 2097–2108. [\[CrossRef\]](#)
- Wang, L.; Good, S.P.; Caylor, K. Global synthesis of vegetation control on evapotranspiration partitioning. *Geophys. Res. Lett.* **2014**, *41*, 6753–6757. [\[CrossRef\]](#)
- Li, X.; Gentine, P.; Lin, C.; Zhou, S.; Sun, Z.; Zheng, Y.; Liu, J.; Zheng, C. A simple and objective method to partition evapotranspiration into transpiration and evaporation at eddy-covariance sites. *Agric. For. Meteorol.* **2019**, *265*, 171–182. [\[CrossRef\]](#)
- Xiu, L.; Yan, C.; Li, X.; Qian, D.; Feng, K. Monitoring the response of vegetation dynamics to ecological engineering in the Mu Us Sandy Land of China from 1982 to 2014. *Environ. Monit. Assess.* **2018**, *190*, 543. [\[CrossRef\]](#)
- Lu, C.; Zhao, T.; Shi, X.; Cao, S. Ecological restoration by afforestation may increase groundwater depth and create potentially large ecological and water opportunity costs in arid and semiarid China. *J. Clean. Prod.* **2018**, *176*, 1213–1222. [\[CrossRef\]](#)
- Gribovszki, Z.; Kalicz, P.; Balog, K.; Szabó, A.; Tóth, T.; Csáfordi, P.; Metwaly, M.; Szalai, S. Groundwater uptake of different surface cover and its consequences in great Hungarian plain. *Ecol. Process.* **2017**, *6*, 39. [\[CrossRef\]](#)
- Yin, L.; Hu, G.; Huang, J.; Wen, D.; Dong, J.; Wang, X.; Li, H. Groundwater-recharge estimation in the Ordos Plateau, China: Comparison of methods. *Hydrogeol. J.* **2011**, *19*, 1563–1575. [\[CrossRef\]](#)
- Doody, T.M.; Benyon, R.G.; Theiveyanathan, S.; Koul, V.; Stewart, L. Development of pan coefficients for estimating evapotranspiration from riparian woody vegetation. *Hydrol. Process.* **2013**, *28*, 2129–2149. [\[CrossRef\]](#)
- Liou, Y.-A.; Kar, S.K. Evapotranspiration Estimation with Remote Sensing and Various Surface Energy Balance Algorithms—A Review. *Energies* **2014**, *7*, 2821–2849. [\[CrossRef\]](#)
- Anapalli, S.S.; Fisher, D.K.; Reddy, K.N.; Wagle, P.; Gowda, P.H.; Sui, R. Quantifying soybean evapotranspiration using an eddy covariance approach. *Agric. Water Manag.* **2018**, *209*, 228–239. [\[CrossRef\]](#)
- White, W. *A Method of Estimating Ground-Water Supplies Based on Discharge by Plants and Evaporation from Soil: Results of Investigations in Escalante Valley*; US Geological Survey: Salt Lake, UT, USA, 1932.
- Cheng, D.-H.; Li, Y.; Chen, X.; Wang, W.-K.; Hou, G.-C.; Wang, C.-L. Estimation of groundwater evapotranspiration using diurnal water table fluctuations in the Mu Us Desert, northern China. *J. Hydrol.* **2013**, *490*, 106–113. [\[CrossRef\]](#)
- Yin, L.; Zhou, Y.; Ge, S.; Wen, D.; Zhang, E.; Dong, J. Comparison and modification of methods for estimating evapotranspiration using diurnal groundwater level fluctuations in arid and semiarid regions. *J. Hydrol.* **2013**, *496*, 9–16. [\[CrossRef\]](#)
- Gribovszki, Z.; Kalicz, P.; Szilágyi, J.; Kucsara, M. Riparian zone evapotranspiration estimation from diurnal groundwater level fluctuations. *J. Hydrol.* **2008**, *349*, 6–17. [\[CrossRef\]](#)
- Wang, T.-Y.; Wang, P.; Yu, J.-J.; Pozdniakov, S.P.; Du, C.-Y.; Zhang, Y.-C. Revisiting the White method for estimating groundwater evapotranspiration: A consideration of sunset and sunrise timings. *Environ. Earth Sci.* **2019**, *78*, 78. [\[CrossRef\]](#)
- Ii, S.P.L. A method for estimating subdaily evapotranspiration of shallow groundwater using diurnal water table fluctuations. *Ecolhydrology* **2008**, *1*, 59–66. [\[CrossRef\]](#)
- Li, N.; Yan, C.; Xie, J. Remote sensing monitoring recent rapid increase of coal mining activity of an important energy base in northern China, a case study of Mu Us Sandy Land. *Resour. Conserv. Recycl.* **2015**, *94*, 129–135. [\[CrossRef\]](#)
- Liang, P.; Yang, X. Landscape spatial patterns in the Maowusu (Mu Us) Sandy Land, northern China and their impact factors. *Catena* **2016**, *145*, 321–333. [\[CrossRef\]](#)
- Cheng, D.-H.; Duan, J.; Qian, K.; Qi, L.; Yang, H.; Chen, X. Groundwater evapotranspiration under psammophilous vegetation covers in the Mu Us Sandy Land, northern China. *J. Arid Land* **2016**, *9*, 98–108. [\[CrossRef\]](#)
- Satchithanantham, S.; Wilson, H.; Glenn, A.J. Contrasting patterns of groundwater evapotranspiration in grass and tree dominated riparian zones of a temperate agricultural catchment. *J. Hydrol.* **2017**, *549*, 654–666. [\[CrossRef\]](#)
- Allen, R.G.; Pereira, L.S.; Raes, D.; Smith, M. *Crop. Evapotranspiration—Guidelines for Computing Crop. Water Requirements*; FAO: Rome, Italy, 1998.
- Schelle, H.; Durner, W.; Iden, S.C.; Fank, J. Simultaneous Estimation of Soil Hydraulic and Root Distribution Parameters from Lysimeter Data by Inverse Modeling. *Procedia Environ. Sci.* **2013**, *19*, 564–573. [\[CrossRef\]](#)

25. Nascimento, Í.V.; de Assis Júnior, R.N.; de Araújo, J.C.; de Alencar, T.L.; Freire, A.G.; Lobato, M.G.R.; da Silva, C.P.; Mota, J.C.A.; Nascimento, C.D.V. Estimation of van Genuchten Equation Parameters in Laboratory and through Inverse Modeling with Hydrus-1D. *J. Agric. Sci.* **2018**, *10*, 102. [[CrossRef](#)]
26. Mavimbela, S.S.W.; Van Rensburg, L.D. Estimating Soil Hydraulic Parameters Characterizing Rainwater Infiltration and Runoff Properties of Dryland Floodplains. *Comput. Water Energy Environ. Eng.* **2019**, *8*, 11–40. [[CrossRef](#)]
27. Šimůnek, J.; Šejna, M.; Saito, H.; Sakai, M.; Genuchten, M.T.V. *The HYDRUS-1D Software Package for Simulating the One-Dimensional Movement of Water, Heat, and Multiple Solutes in Variably-Saturated Media*; Version 4.17, HYDRUS Software Series 3; Department of Environmental Sciences, University of California Riverside: Riverside, CA, USA, 2013.
28. Li, Y.; Šimůnek, J.; Jing, L.; Zhang, Z.; Ni, L. Evaluation of water movement and water losses in a direct-seeded-rice field experiment using Hydrus-1D. *Agric. Water Manag.* **2014**, *142*, 38–46. [[CrossRef](#)]
29. Ritchie, J.T. Model for predicting evaporation from a row crop with incomplete cover. *Water Resour. Res.* **1972**, *8*, 1204–1213. [[CrossRef](#)]
30. Belmans, C.; Wesseling, J.; Feddes, R. Simulation model of the water balance of a cropped soil: SWATRE. *J. Hydrol.* **1983**, *63*, 271–286. [[CrossRef](#)]
31. Zeng, X. Global Vegetation Root Distribution for Land Modeling. *J. Hydrometeorol.* **2001**, *2*, 525–530. [[CrossRef](#)]
32. van Genuchten, M.T. *A Numerical Model for Water and Solute Movement in and below the Root Zone*; Unpublished Report; U.S. Salinity Laboratory, USDA, ARS: Riverside, CA, USA, 1987.
33. Willmott, C.J.; Ackleson, S.G.; Davis, R.E.; Feddema, J.J.; Klink, K.M.; LeGates, D.R.; O'Donnell, J.; Rowe, C.M. Statistics for the evaluation and comparison of models. *J. Geophys. Res. Space Phys.* **1985**, *90*, 8995–9005. [[CrossRef](#)]
34. Nash, J.E.; Sutcliffe, J.V. River flow forecasting through conceptual models part I-A discussion of principles. *J. Hydrol.* **1970**, *10*, 282–290. [[CrossRef](#)]
35. LeGates, D.R.; McCabe, G.J., Jr. Evaluating the use of “goodness-of-fit” Measures in hydrologic and hydroclimatic model validation. *Water Resour. Res.* **1999**, *35*, 233–241. [[CrossRef](#)]
36. Laczniak, R.J.; Smith, J.L.; Elliott, P.E.; DeMeo, G.A.; Chatigny, M.A.; Roemer, G.J. *Ground-Water Discharge Determined from Estimates of Evapotranspiration, Death Valley Regional Flow System, Nevada and California*; Report 2001-4195; U.S. Geological Survey: Reston, VA, USA, 2001.
37. Nachabe, M.H. Analytical expressions for transient specific yield and shallow water table drainage. *Water Resour. Res.* **2002**, *38*, 11-1–11-7. [[CrossRef](#)]
38. Li, S.P.L.; Butler, J.J., Jr.; Gorelick, S.M. Estimation of groundwater consumption by phreatophytes using diurnal water table fluctuations: A saturated-unsaturated flow assessment. *Water Resour. Res.* **2005**, *41*, 1–14. [[CrossRef](#)]
39. Gribovszki, Z. Comparison of specific-yield estimates for calculating evapotranspiration from diurnal groundwater-level fluctuations. *Hydrogeol. J.* **2017**, *26*, 869–880. [[CrossRef](#)]
40. Freeze, R.A.; Cherry, J.A. *Groundwater*; Prentice-Hall, Inc.: Englewood Cliffs, NJ, USA, 1979.
41. Duke, H.R. Capillary Properties of Soils-Influence upon Specific Yield. *Trans. ASAE* **1972**, *15*, 0688–0691. [[CrossRef](#)]
42. Butler, J.J.; Kluitenberg, G.J.; Whittemore, D.O.; Li, S.P.L.; Jin, W.; Billinger, M.A.; Zhan, X. A field investigation of phreatophyte-induced fluctuations in the water table. *Water Resour. Res.* **2007**, *43*, 299–309. [[CrossRef](#)]
43. Yue, W.; Wang, T.; Franz, T.E.; Chen, X. Spatiotemporal patterns of water table fluctuations and evapotranspiration induced by riparian vegetation in a semiarid area. *Water Resour. Res.* **2016**, *52*, 1948–1960. [[CrossRef](#)]
44. Hughes, C.; Kalma, J.D.; Binning, P.J.; Willgoose, G.R.; Vertzonis, M. Estimating evapotranspiration for a temperate salt marsh, Newcastle, Australia. *Hydrol. Process.* **2001**, *15*, 957–975. [[CrossRef](#)]
45. Senitz, S. Untersuchung und Anwendung kurzperiodischer Schwankungen des Grundwasserspiegels in Thüringen. *Grundwasser* **2001**, *6*, 163–173. [[CrossRef](#)]
46. Jiang, X.-W.; Sun, Z.-C.; Zhao, K.-Y.; Shi, F.-S.; Wan, L.; Wang, X.; Shi, Z. A method for simultaneous estimation of groundwater evapotranspiration and inflow rates in the discharge area using seasonal water table fluctuations. *J. Hydrol.* **2017**, *548*, 498–507. [[CrossRef](#)]
47. Scott, M.L.; Lines, G.C.; Auble, G.T. Channel incision and patterns of cottonwood stress and mortality along the Mojave River, California. *J. Arid Environ.* **2000**, *44*, 399–414. [[CrossRef](#)]
48. Martín, D.; Chambers, J. Restoration of riparian meadows degraded by livestock grazing: Above- and belowground responses. *Plant Ecol.* **2002**, *163*, 77–91. [[CrossRef](#)]
49. Shah, N.; Nachabe, M.; Ross, M. Extinction Depth and Evapotranspiration from Ground Water under Selected Land Covers. *Groundwater* **2007**, *45*, 329–338. [[CrossRef](#)] [[PubMed](#)]